TOP QUARK PRODUCTION NEAR THRESHOLD AT NLC [a]

OLEG YAKOVLEV
Randall Laboratory of Physics, University of Michigan, Ann Arbor, Michigan 48109-1120, USA

STEFAN GROOTE
Institut für Physik der Johannes-Gutenberg-Universität, Staudinger Weg 7, D-55099 Mainz, Germany

Floyd R. Newman Laboratory, Cornell University, Ithaca, NY 14853, USA

In this talk we discuss the process $e^+e^- \to t\bar{t}$ near threshold. In particular we discuss a quark mass definition which is a generalization of the static PS mass. The new definition allows us to calculate recoil corrections to the static PS mass. Using this result we calculate the cross section of $e^+e^- \to t\bar{t}$ near threshold at NNLO accuracy adopting three alternative approaches, namely (1) fixing the pole mass, (2) fixing the PS mass, and (3) fixing the new mass which we call the $\overline{\text{PS}}$ mass. We demonstrate that perturbative predictions for the cross section become much more stable if we use the PS or the $\overline{\text{PS}}$ mass for the calculations. A careful analysis suggests that the top quark mass can be extracted from a threshold scan at NLC with an accuracy of about $100 - 200\,\text{MeV}$.

(Preprint: UM-TH-00-22, CLNS 00/1690)

1 Introduction

1.1 On NLC, FMC, LHC and Tevatron

The top quark physics will be one of the main subject of future e^+e^- and $\mu^+\mu^-$ colliders such as the Next Linear Collider (NLC) and the Future Muon Collider (FMC). The goals are to measure and to determine the properties of the top quark which was first discovered at the Tevatron [1] with a mass of $m = 174.3 \pm 5\,\text{GeV}$ [2]. Although the top quark will be studied at the LHC and the Tevatron (RUN-II) with an expected accuracy for the mass of $2 - 3\,\text{GeV}$, the *most accurate measurement* of the mass with an accuracy of 0.1% ($100 - 200\,\text{MeV}$) is expected to be obtained only at the NLC [3].

[a] Talk given by O.Yakovlev at the Conference “PHENOMENOLOGY-2000”, Madison, Wisconsin, April 15-17, 2000

1.2 *Why do we need 10^{-3} accuracy in the top mass?*

The top quark mass enters the relation between the electroweak precision observables indirectly through loops effects. The global electro-weak fit of the Standard Model requires to have very accurate input data in order to make a constraint for the masses of undiscovered particles, such as the Higgs boson or other particles. The increase in the accuracy of the top quark mass will improve the limits on the Higgs mass. In addition we can study possible deviations from the Standard Model through anomalous couplings, CP violation, or extra dimensions.

1.3 *LO and NLO cross section*

Due to the large top quark width, the top-antitop pair cannot hadronize into toponium resonances. The cross section appears therefore to have a smooth line-shape showing only a moderate $1S$ peak. In addition the top quark width serves as an infrared cutoff [4,5] and as a natural smearing over the energy [6]. As a result, the nonperturbative QCD effects induced by the gluon condensate are small [7,8], allowing us to calculate the cross section with high accuracy by using perturbative QCD even in the threshold region. Many theoretical studies at LO and NLO have been done in the past for the total cross section [4,5,7,9], for the momentum distribution [10,11], also accounting for electro-weak corrections [12,13,14], and for the complete NLO correction including non-factorizable corrections [15,16,17,18]. It was proven that the non-factorizable corrections cancel in the inclusive cross section at NLO [15,16,17,19,20,21].

1.4 *On NNLO results*

Recently, the NNLO analysis of the inclusive threshold production cross section has been reported [22,23,24,25,26,27,28]. The results of the NNLO analysis are summarized in a review article [29]. To summarize the results for a standard approach using the pole mass, the NNLO corrections are uncomfortably large, spoiling the possibility for the top quark mass extraction at NLC with good accuracy because the $1S$ peak is shifted by about $0.5\,\mathrm{GeV}$ by the NNLO, the last known correction. One of the main reasons for this is the usage of the pole mass in the calculations. It was realized that such type of instability is caused by the fact that the pole mass is a badly defined object within full QCD [30,31].

In this talk we discuss a definition of the quark mass alternative to the pole mass. It is the so-called potential subtracted (PS) mass, suggested in Ref. [32]. In contrast to the pole mass the PS mass is not sensitive to the non-perturbative QCD effects. We derive recoil corrections to the relation of the pole mass to the PS mass and demonstrate that perturbative predictions for the cross section become much more stable at higher orders of QCD (shifts are below 0.1 GeV) if we use the PS mass for the calculations. This understanding removes one of the obstacles for the accurate top quark mass measurement and it can be expected that the top quark mass will be extracted from a threshold scan at NLC with an accuracy of about $100 - 200\,\mathrm{MeV}$. We have to mention that the necessity of isolating the IR contributions in the mass calculation and the consideration of a short distance mass have been studied intensively [31,32,33,34,35]. The applications of the PS, LS and $1S$ mass have been reported recently by several groups [25,26,27,36,37] and reviewed in Ref. [29]. The detailed comparison of our results using the PS mass with results of other groups have been performed in Ref. [29] so that we refer the reader to this reference for details.

In this talk we review Ref. [38]. In particular, we discuss a quark mass definition (we call it $\overline{\mathrm{PS}}$ mass) which is a generalization of the static PS mass proposed by M. Beneke [32]. The new definition allows us to calculate recoil corrections to the static PS mass. Second, we calculate the cross section for $e^+e^- \to t\bar{t}$ near threshold with NNLO accuracy using three alternative mass schemes, i.e. (1) the pole mass, (2) the static PS mass, and (3) the new $\overline{\mathrm{PS}}$ mass. The results of the first approach has already been reported in Ref. [24], the results for the top quark pair production near threshold using the static PS mass were presented in Refs. [36,37,38,29], the third alternative schemes were discussed in Refs. [38].

2 Top quark production near threshold with NNLO accuracy

In this section we consider the cross section of the process $e^+e^- \to t\bar{t}$ in the near threshold region where the velocity v of the top quark is small. It is well known that the conventional perturbative expansion does not work in the non-relativistic region because of the presence of the Coulomb singularities at small velocities $v \to 0$. The terms proportional to $(\alpha_s/v)^n$ appear due to the instantaneous Coulomb interaction between the top and the antitop quark. The standard technique for re-summing the terms $(\alpha_s/v)^n$ consists in using the Schrödinger equation for the Coulomb potential and in finding the Green function [4,5]. The Green function is then related to the cross section by the optical theorem. In order to determine NLO corrections to the cross section we need to know the short-distance correction to the vector current [39], the NLO correction to the Coulomb potential [40], and the contribution of the non-factorizable corrections [15,16,17]. It was proven that the non-factorizable corrections cancel in the inclusive cross section at NLO and beyond [15,16,17,19,20,21]. At NNLO the situation is more complicated. One of the obstacles for a straightforward calculation are the UV divergences coming from relativistic corrections to the Coulomb potential. This problem can be solved by a proper factorization of the amplitudes and by employing effective theories. We want to sketch the derivation of the inclusive cross section. The inclusive cross section can be obtained from the correlation function of two vector currents $j_\mu(x) = \bar{t}(x)\gamma_\mu t(x)$,

$$\Pi_{\mu\nu}(p^2) = i\int d^4x e^{ip\cdot x}\langle 0|T\{j_\mu(x), j_\nu(0)\}|0\rangle. \tag{1}$$

The first step is to expand the Lagrangian and the currents

$$j_i = \bar{t}\gamma_i t = c_1\psi^\dagger\sigma_i\chi - \frac{c_2}{6m^2}\psi^\dagger\sigma_i(i\mathbf{D})^2\chi \tag{2}$$

consistently in $1/m$. The useful language for treating the one and two non-relativistic quark(s) is provided by the NRQCD [41,42] and the PNRQCD [43], respectively. After the expansion, the cross section reads

$$\begin{aligned}
R &= \sigma(e^+e^- \to t\bar{t})/\sigma_{pt} \\
&= e_Q^2 N_c \frac{24\pi}{s} C(r_0) \mathrm{Im}\left[\left(1 - \frac{\vec{p}^{\,2}}{3m^2}\right) G(r_0, r_0|E + i\Gamma)\right]\Bigg|_{r_0\to 0}
\end{aligned} \tag{3}$$

where $\sigma_{pt} = 4\pi\alpha^2/3s$, e_Q is the electric charge of the top quark, N_c is the number of colors, $\sqrt{s} = 2m + E$ is the total center-of-mass energy of the quark-antiquark system, m is the top quark pole mass and Γ is the top quark width. The unknown coefficient $C(r_0)$ can be fixed by using a direct QCD calculation of the vector vertex at NNLO in the so-called intermediate region [44,45] and by using the direct matching procedure suggested in Ref. [46].

The function $G(\vec{r}, \vec{r}\,'|E + i\Gamma)$ is the non-relativistic Green function. It satisfies the Schrödinger equation

$$(H - E - i\Gamma)G(\vec{r}, \vec{r}\,'|E + i\Gamma) = \delta(\vec{r} - \vec{r}\,'), \tag{4}$$

H is the non-relativistic Hamiltonian of the heavy quark-antiquark system. It is shown [22,23,24] that the Schrödinger equation can be reduced to the equation

$$(H_1 - E_1)G_1(r, r'|E_1) = \delta^3(r - r') \tag{5}$$

with the energy $E_1 = \bar{E} + \bar{E}^2/4m$, $\bar{E} = E + i\Gamma$, and with the Hamiltonian

$$H_1 = \frac{\vec{p}^{\,2}}{m} + V_C(r) + \frac{3\bar{E}}{2m}V_0(r) - \left(\frac{2}{3} + \frac{C_A}{C_F}\right)\frac{V_0^2(r)}{2m},$$

$$
\begin{aligned}
V_0(r) &= -\frac{\alpha_s(\mu)C_F}{r}, \\
V_C(r) &= V_0(r)\Bigg\{1+\frac{\alpha_s(\mu)C_F}{4\pi}\left(2\beta_0\ln(\mu' r)+a_1\right) \qquad (6)\\
&+\left(\frac{\alpha_s(\mu)}{4\pi}\right)^2\left(\beta_0^2\left(4\ln^2(\mu' r)+\frac{\pi^2}{3}\right)+2(\beta_1+2\beta_0 a_1)\ln(\mu' r)+a_2\right)\Bigg\}
\end{aligned}
$$

where $\mu' = \mu e^{\gamma_E}$, μ is the renormalization scale, and γ_E is Euler's constant. The QCD beta function coefficients β_0 and β_1 and the coefficients a_1 and a_2 are listed later this talk. The final expression for the NNLO cross section is given by

$$
\begin{aligned}
R^{\mathrm{NNLO}}(E) = \frac{8\pi}{m^2}\left\{1-4C_F\frac{\alpha_s(m)}{\pi}+C_2(r_0)C_F\left(\frac{\alpha_s(m)}{\pi}\right)^2\right\} \times \\
\times \operatorname{Im}\left[\left(1-\frac{5\bar{E}}{6m}\right)G_1(r_0,r_0|E_1)\right] \qquad (7)
\end{aligned}
$$

with $G_1(r_0,r_0|E_1)$ being the solution of Eq. (5) at $r=r'=r_0$. For the numerical solution we use the program derived in Ref. [24] by one of the authors.

3 On the mass definitions

The top quark mass is an input parameter of the Standard Model. Although it is widely accepted that the quark masses are generated due to the Higgs mechanism, the value of the mass cannot be calculated from the Standard Model. Instead, quark masses have to be determined from the comparison of theoretical predictions and experimental data.

It is important to stress that there is no unique definition of the quark mass. Because the quark cannot be observed as a free particle like the electron, the quark mass is a purely theoretical notion and depends on the concept adopted for its definition. The best known definitions are the pole mass and the $\overline{\mathrm{MS}}$ mass. However, both definitions are not adequate for the analysis of top quark production near threshold. The pole mass should not be used because it has the renormalon ambiguity and cannot be determined more accurately than $300-400\,\mathrm{MeV}$ [30,31] (see also Refs. [32,47,48]). Actually, we may relate the pole mass with some short distance mass like the $\overline{\mathrm{MS}}$ mass M which for the "large β_0 approximation" (see e.g. Ref. [49]) is given by

$$
m_{\mathrm{pole}} = M\left\{1+\sum m_n\left(\frac{\beta_0\alpha_s}{4\pi}\right)^n\right\}. \qquad (8)
$$

The Borel image of the pole mass $m_{\rm pole}$ reads

$$\bar{m}_{\rm pole}(u) = \sum m_n \frac{u^n}{n!} \tag{9}$$

The function $m_{\rm pole}(u) \sim \Gamma(1-2u)$ has poles at real and positive values $u = 1/2, 3/2, \ldots$. Therefore, the inverse Borel transformation

$$m_{\rm pole} = \int du \exp\left(\frac{4\pi u}{\beta_0 \alpha_s}\right) \bar{m}_{\rm pole}(u) \tag{10}$$

generates ambiguities of the order

$$\delta m \approx \exp\left(\frac{4\pi}{\beta_0 \alpha_s}\right) \approx \Lambda_{\rm QCD}. \tag{11}$$

These ambiguities are known in the literature as renormalon ambiguities (see for example Refs. [50,51]).

The $\overline{\rm MS}$ mass is an Euclidean mass, defined at high virtuality, and therefore destroys the non-relativistic expansion. Instead, it was recently suggested to use threshold masses like the low scale (LS) mass [31], the potential subtracted (PS) mass [32], or one half of the perturbative mass of a fictious 1^3S_1 ground state (called $1S$ mass) [26]. In this talk we focus on the PS mass suggested in Ref. [32],

$$m_{\rm PS} = m_{\rm pole} - \delta m_{\rm PS} \quad \text{with} \quad \delta m_{\rm PS} = -\frac{1}{2} \int^{|\vec{k}|<\mu_f} \frac{d^3k}{(2\pi)^3} V_C(|\vec{k}|) \tag{12}$$

where V_C is the quark-antiquark Coulomb potential.

3.1 On renormalons and soft QCD effects cancellation

In order to understand why this mass is better defined than the pole mass and to see that the pole mass is very sensitive to long distance effects, it is enough to consider the one-loop expression for the self energy diagram. Taking the residue in k_0, one obtains a soft self energy contribution which comes from momenta k with $|\vec{k}| < \Lambda_{\rm QCD}$,

$$\delta m = 4\pi \alpha_s C_F \int\limits_{|\vec{k}|<\Lambda_{\rm QCD}} \frac{d^3k}{(2\pi)^3} \frac{1}{2|\vec{k}|^2} = \frac{\alpha_s C_F}{\pi} \Lambda_{\rm QCD}. \tag{13}$$

We observe that the pole mass has a non-perturbative uncertainty of order $\Lambda_{\rm QCD}$ which then penetrates into consequent perturbative QCD calculations.

This uncertainty or ambiguity is caused by the poles of the Borel transformation as shown before. However, it is easy to realize that the PS mass is free of this ambiguity. Indeed, the term δm in Eq. (13) and therefore the renormalon ambiguities associated with it cancel in the definition of the PS mass as given in Eq. (12) as well as in the combination $2m_{\rm pole} + V(r)$ which is known as static energy. We can see this by applying the Borel technique also to the QCD potential

$$V(r) = \int \frac{d^3k}{(2\pi)^3} \left(-\frac{4\pi C_F \alpha_s(k^2)}{k^2} \right) e^{ik\cdot r}. \tag{14}$$

The Borel image of the potential $V(r) = \sum V_n(\beta_0\alpha_s/4\pi)^n$ in the "large β_0 limit" is given by

$$\bar{V}(u) = \sum V_n \frac{u^n}{n!}. \tag{15}$$

with the function $\bar{V}(u) \sim \Gamma(1-2u)$ having again poles at real and positive values $u = 1/2, 3/2, \ldots$. The inverse Borel transformation

$$V(r) = \int du \exp\left(\frac{4\pi u}{\beta_0\alpha_s}\right) \bar{V}(u). \tag{16}$$

generates ambiguities of the order

$$\delta V(r) \approx \exp\left(\frac{4\pi}{\beta_0\alpha_s}\right) \approx \Lambda_{\rm QCD}. \tag{17}$$

The coefficient in $\bar{V}(u)$ differs from $\bar{m}_{\rm pole}(u)$ by a factor -2. Therefore we observe the cancellation of the renormalon ambiguity in the combination $2m_{\rm pole}+V(r)$ [32,50,47].

The definition in Eq. (12) has been given in Ref. [32] but has already been discussed implicitly in Ref. [31]. The remarkable step made in Ref. [32] is to use this definition beyond one-loop order. It has been proven in Ref. [32] that the cancellation of the infrared QCD contributions to the PS mass in Eq. (12) holds even at higher loop orders. Still the definition in Eq. (12) is valid only in the static approximation and does not contain $1/m$ corrections like the other threshold mass definitions. We therefore suggest to extend the definition given in Ref. [32].

3.2 The $\overline{\rm PS}$ *mass definition*

Our objective is that the definition should be gauge independent and well-defined within quantum field theory so that radiative and relativistic correc-

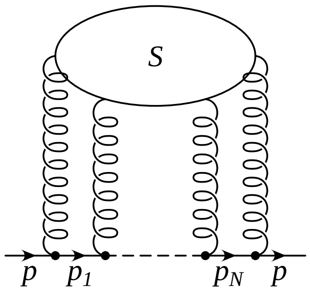

Figure 1: The general structure of the self energy diagram of a quark

tions can be calculated in a systematic way. Our definition is given by

$$m_{\overline{\rm PS}} = m_{\rm pole} - \delta m_{\overline{\rm PS}} \quad \text{with} \quad \delta m_{\overline{\rm PS}} = \Sigma_{\rm soft}(\not p)\Big|_{\not p=m}, \tag{18}$$

where $\Sigma_{\rm soft}$ is the soft part of the heavy quark self energy which is defined as the part where at least one of the heavy quark propagators is on-shell. Starting point for our considerations is therefore the self energy of an on-shell quark with mass m and momentum p (i.e. $p^2 = m^2$) as shown in Fig. 1 and written down as

$$\begin{aligned} -i\Sigma(\not p) = \int \prod_{m=1}^{M} \frac{d^4 l_m}{(2\pi)^4} S^{\{a_n\}}_{\{\alpha_n\}}(\{l_m\}) \left(-ig_s \gamma^{\alpha_{N+1}} T_{a_{N+1}}\right) \; \times \\ \times \prod_{n=N}^{1} \frac{i}{\not p_n - m} \left(-ig_s \gamma^{\alpha_n} T_{a_n}\right) \end{aligned} \tag{19}$$

where the last factor is a non-commutative product with decreasing index n. The line momenta k_n are linear combinations of the gluon loop momenta l_m, the particular representation is specified by the structure S. The symbol $\{l_m\}$ means the set of all these loop momenta, the same symbol is used for the Lorentz and color indices. In general we have $M \leq N$ which means that line momenta can be correlated. The momenta of the virtual quark states are given by $p_n = p + k_n$.

The quark is considered to be at rest, $p = (m, \vec{0})$, and it interacts with a number of gluons. The subdiagram S displayed in Fig. 1 describes the interaction between the gluons. In general the quark lines between the interaction points represent virtual quark states. However, if the virtual quark comes very close to the mass shell and the total momentum of the cloud of virtual gluons becomes soft, this situation gives rise to long-distance nonperturbative QCD interactions. The described (virtual) contributions results in the soft part of the self energy, $\Sigma_{\rm soft}$. So we define

$$
\begin{aligned}
-i\Sigma_{\rm soft}(\not p) \;&=\; \sum_{i=1}^{N}\int\prod_{m=1}^{M}\frac{d^4l_m}{(2\pi)^4}S^{\{a_n\}}_{\{\alpha_n\}}(\{l_m\})\left(-ig_s\gamma^{\alpha_{N+1}}T_{a_{N+1}}\right)\;\times \\
&\times\prod_{n=N}^{i+1}\frac{i}{\not p_n-m}\left(-ig_s\gamma^{\alpha_n}T_{a_n}\right)i(\not p_i+m)\left(-i\pi\delta(p_i^2-m^2)\right)\;\times \\
&\times\;\left(-ig_s\gamma^{\alpha_i}T_{a_i}\right)\prod_{n=i-1}^{1}\frac{i}{\not p_n-m}\left(-ig_s\gamma^{\alpha_n}T_{a_n}\right). \qquad (20)
\end{aligned}
$$

One can derive this expression from Eq. (19) by using the identity

$$
\frac{1}{p^2-m^2+i\epsilon}=-i\pi\delta(p^2-m^2)+P\left(\frac{1}{p^2-m^2}\right) \qquad (21)
$$

and the fact that the principal value integral does not give any infrared sensitive contribution. The delta function can be used to remove the integration over the zero component of k_i. In order to parameterize the softness of the gluon cloud we impose a cutoff on the spatial component, $|\vec{k}_i|<\mu_f$, and indicate this by a label μ_f written at the upper limit of the three-dimensional integral. This cutoff μ_f is also known as *factorization scale*. So we can rewrite Eq. (20) as

$$
\Sigma_{\rm soft}(\not p,\mu_f)=-\frac{1}{2}\sum_{i=1}^{N}\int^{\mu_f}\frac{d^3k_i}{(2\pi)^3}V(\vec{k}_i,p) \qquad (22)
$$

where

$$
\begin{aligned}
V(\vec{k}_i,p) \;&=\; -\int\prod_{m=1}^{M-1}\frac{d^4l_m}{(2\pi)^4}S^{\{a_n\}}_{\{\alpha_n\}}(\{l_m\})\;\times \\
&\times\;\left(-ig_s\gamma^{\alpha_{N+1}}T_{a_{N+1}}\right)\prod_{n=N}^{i+1}\frac{i}{\not p_n-m}\left(-ig_s\gamma^{\alpha_n}T_{a_n}\right)\frac{\not p_i+m}{2p_i^0}\;\times \\
&\times\;\left(-ig_s\gamma^{\alpha_i}T_{a_i}\right)\prod_{n=i-1}^{1}\frac{i}{\not p_n-m}\left(-ig_s\gamma^{\alpha_n}T_{a_n}\right). \qquad (23)
\end{aligned}
$$

The range of the index m is reduced by one which indicates that one of the loop momenta is extracted as line momentum of the i-th line. In the following

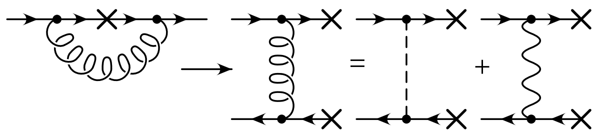

Figure 2: Leading order contribution to the quark self energy (a) and to the quark-antiquark potential (b). The cross indicates the point where we cut the quark line by imposing an on-shell condition to the virtual quark state. The gluon propagator can be decomposed in a Coulomb propagator (c) and a transverse propagator (d).

we deal with the different realizations of this compact expression. As we will see explicitly, the function $V(\vec{k},p)$ occurring as integrand can be seen as quark-antiquark potential where we have summed over the spin of the tensor product of a final state with an initial state. Because the static quark-antiquark potential is used in a similar way in Ref. [32], we recover the result of Ref. [32] in the static limit.

3.3 The one-loop contribution

The leading order contribution to the self energy of the quark is given by

$$\Sigma(\not{p}) = i\int\frac{d^4k}{(2\pi)^4}(-ig_s\gamma_\alpha T_a)\frac{i}{\not{p}+\not{k}-m}(-ig_s\gamma^\alpha T_a)\frac{-i}{k^2} \tag{24}$$

where Feynman gauge is used for the gluon. The soft part of it is given by

$$\Sigma_{\rm soft}(\not{p},\mu_f) = -\frac{1}{2}\int^{\mu_f}\frac{d^3k}{(2\pi)^3}V(\vec{k},p), \quad V(\vec{k},p) = V_+(\vec{k},p)+V_-(\vec{k},p) \tag{25}$$

where

$$V_\pm(\vec{k},p) = -\frac{g_s^2C_F(\sqrt{m^2+\kappa^2}\mp 2m)}{2m\sqrt{m^2+\kappa^2}(\sqrt{m^2+\kappa^2}-m)} \tag{26}$$

and $\kappa=|\vec{k}|$. The procedure of taking the soft part by setting a cut is shown in Fig. 2(a–b). The two potential parts are known as the scattering potential $V_+(\vec{k},p)$ and the annihilation potential $V_-(\vec{k},p)$ and correspond to the two zeros $k_\pm = \pm\sqrt{\kappa^2+m^2}-m$ of the delta function. Integrating the potential up to the factorization scale μ_f, we obtain

$$\Sigma_{\rm soft}(\mu_f) = \frac{\alpha_sC_F}{2\pi}m\left\{3\ln\left(\frac{\mu_f}{m}+\sqrt{\frac{\mu_f^2}{m^2}+1}\right)-\frac{\mu_f}{m}\sqrt{\frac{\mu_f^2}{m^2}+1}\right\}. \tag{27}$$

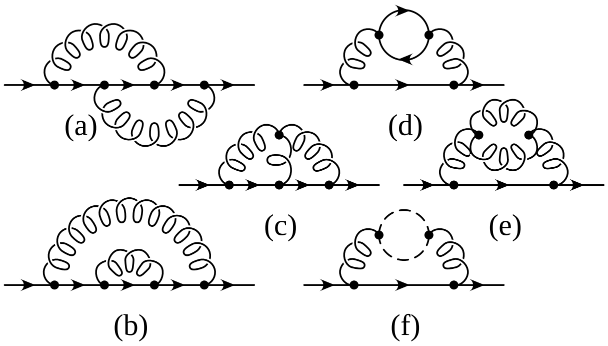

Figure 3: Two-loop contributions to the quark self energy

The expansion of this expression in small values of μ_f/m results in

$$\Sigma_{\rm soft}(\mu_f) = \frac{\alpha_s C_F}{\pi}\mu_f \left\{1 - \frac{\mu_f^2}{2m^2}\right\}. \tag{28}$$

The first term reproduces the result given in Ref. [32] to leading order in α_s while the second term is the recoil correction to the static limit in this order of perturbation theory. This second term is related to the Breit-Fermi potential but does not coincide with it.

3.4 Two loop contributions

To take a step beyond the leading order perturbation theory, we consider two-loop diagrams for the heavy quark self energy as shown in Fig. 3. We calculate them in Coulomb gauge, even though we stress that our final result is gauge invariant. The gluon propagator in Coulomb gauge is given by

$$G_{00}^{ab}(k) = \frac{i\delta^{ab}}{\vec{k}^{\,2}}, \qquad G_{ij}^{ab}(k) = \frac{i\delta^{ab}}{k^2}\left(\delta_{ij} - \frac{k_i k_j}{\vec{k}^{\,2}}\right), \qquad i,j = 1,2,3. \tag{29}$$

The use of Coulomb gauge splits up the gluon propagators into a Coulomb term (Coulomb gluon) and a transverse term (transverse gluon) where the first one couples to the quark via the time components only. This splitting is shown in Fig. 2(b–d).

In cutting the quark line in all possible ways we obtain a lot of diagrams from the ones shown in Fig. 3. However, we find that the final contribution of the two abelian diagrams in Fig. 3(a–b) to the soft part of the self energy is suppressed by μ_f^2/m^2. Therefore it turns out that the only abelian diagrams which can give a non-suppressed contribution to the soft part of the quark self energy are the diagrams containing the vacuum polarization of the gluon as shown in Fig. 3(d–f). The simple calculation of these diagrams within the $\overline{\mathrm{MS}}$ scheme, accounting only for light fermion loops, gluon loop (and ghost loop if Feynman gauge is used) results after renormalization in

$$\begin{aligned}
\Sigma^A_{\rm soft} &= -\frac{1}{2}\int\frac{d^3k}{(2\pi)^3}\left(\frac{4\pi C_F\alpha_s(\mu)}{|\vec{k}|^2}\right) \times \\
&\quad\times \left\{1+\frac{\alpha_s}{4\pi}\left(\frac{31C_A}{9}-\frac{20T_FN_F}{9}-\left(\frac{11C_A}{3}-\frac{4T_FN_F}{3}\right)\ln\left(\frac{|\vec{k}|^2}{\mu^2}\right)\right)\right\} \\
&= \frac{\alpha_S(\mu)C_F}{\pi}\mu_f\left\{1+\frac{\alpha_s(\mu)}{4\pi}\left(a_1-\beta_0\ln\left(\frac{\mu_f^2}{\mu^2}\right)\right)\right\}. \qquad (30)
\end{aligned}$$

This result has been anticipated because the expression in the curly brackets of the integrand reproduces the next-to-leading order correction to the QCD Coulomb potential.

For the only non-abelian diagram in Fig. 3(c) the use of Coulomb gauge leads to seven diagrams. However, direct calculations show that only the diagram where the transverse gluon is joined by Coulomb gluons on both sides of the quark line contributes to the order $g_s^4\mu_f/m$. For this diagram and therefore for the whole non-abelian contribution up to this order we obtain

$$\Sigma^{NA}_{\rm soft} = \frac{\alpha_s^2 C_F C_A}{8m}\mu_f^2. \qquad (31)$$

This result has been anticipated, too, to be minus one half of the non-abelian correction to the QCD Coulomb potential, which is known in the literature (see for example Refs. [52,53]),

$$\Sigma^{NA}_{\rm soft} = -\frac{1}{2}\int^{\mu_f}\frac{d^3k}{(2\pi)^3}\left\{-\frac{\pi^2\alpha_s^2C_FC_A}{m|\vec{k}|}\right\} = \frac{\alpha_s^2C_FC_A}{8m}\mu_f^2. \qquad (32)$$

3.5 Our final result

Summarizing all contribution up to NNLO accuracy, we obtain

$$m_{\overline{\rm PS}}(\mu_f) - m = -\frac{\alpha_s(\mu)C_F}{\pi}\mu_f\left\{1 + C_0'\frac{\mu_f}{m} + C_0''\frac{\mu_f^2}{m^2}\right.$$

$$
+\frac{\alpha_s(\mu)}{4\pi}\left(C_1 + C_1'\frac{\mu_f}{m}\right) + C_2\left(\frac{\alpha_s(\mu)}{4\pi}\right)^2 \Bigg\} \tag{33}
$$

where m is the pole mass, μ is the renormalization scale, μ_f is the factorization scale, and

$$
\begin{aligned}
C_0 &= 1, \qquad C_0' \;=\; 0, \qquad C_0'' \;=\; -\frac{1}{2}, \\
C_1 &= a_1 - 2\beta_0 \ln\left(\frac{\mu_f}{\mu}\right), \qquad C_1' \;=\; C_A\frac{\pi^2}{2}, \\
C_2 &= a_2 - 2(2a_1\beta_0 + \beta_1)\left(\ln\left(\frac{\mu_f}{\mu}\right) - 1\right) \\
&\quad +4\beta_0^2\left(\ln^2\left(\frac{\mu_f}{\mu}\right) - 2\ln\left(\frac{\mu_f}{\mu}\right) + 2\right).
\end{aligned} \tag{34}
$$

The constants a_1 and a_2 are given by [54,55,56]

$$
\begin{aligned}
a_1 &= \frac{31}{9}C_A - \frac{20}{9}T_F N_F, \\
a_2 &= \left(\frac{4343}{162} + 4\pi^2 - \frac{\pi^4}{4} + \frac{22}{3}\zeta_3\right)C_A^2 - \left(\frac{1798}{81} + \frac{56}{3}\zeta_3\right)C_A T_F N_F \\
&\quad + \left(\frac{20}{9}T_F N_F\right)^2 - \left(\frac{55}{3} - 16\zeta_3\right)C_F T_F N_F,
\end{aligned} \tag{35}
$$

the coefficients of the beta function are known as

$$
\beta_0 = \frac{11}{3}C_A - \frac{4}{3}N_F T_F, \quad \beta_1 = \frac{34}{3}C_A^2 - \frac{20}{3}C_A T_F N_F - 4C_F T_F N_F \tag{36}
$$

where $C_F = 4/3$, $C_A = 3$ and $T_F = 1/2$ are color factors and $N_F = 5$ is the number of light flavors. The coefficients C_1 and C_2 in Eq. (33) have been derived in Ref. [32] by using known corrections to the QCD potential. In this work we have derived the coefficients C_0', C_0'', and C_1'. Note that our result can be represented in a condensed form as

$$
m_{\overline{\mathrm{PS}}}(\mu_f) - m = -\frac{1}{2}\int^{\mu_f}\frac{d^3k}{(2\pi)^3}\left(V_C(|\vec{k}|) + V_R(|\vec{k}|) + V_{NA}(|\vec{k}|)\right) \tag{37}
$$

where the first term V_C is the static Coulomb potential, V_R is the relativistic correction (which is related to Breit-Fermi potential but does not coincide with it), and V_{NA} is the non-abelian correction. Note that we did not include electroweak corrections neither in this mass relation nor in the cross section we will look on later. Finally (which is actually *not* our result) the relation between the pole mass and the $\overline{\rm MS}$ mass is given by the three-loop relation [57,58]

$$\frac{m_{\rm pole}}{\overline{m}(\overline{m})} = 1 + \frac{4}{3}\left(\frac{\alpha_s}{\pi}\right) + \left(\frac{\alpha_s}{\pi}\right)^2 (-1.0414 N_F + 13.4434) + \left(\frac{\alpha_s}{\pi}\right)^3 (0.6527 N_F^2 - 26.655 N_F + 190.595) \qquad (38)$$

where $\alpha_s = \alpha_s(\overline{m})$ is taken at the $\overline{\rm MS}$ mass.

Using the relations between the masses, we fix the $\overline{\rm MS}$ mass to take the values $\overline{m}(\overline{m}) = 160\,{\rm GeV}$, $165\,{\rm GeV}$, and $170\,{\rm GeV}$ and use Eq. (38) to determine the pole mass at LO, NLO, and NNLO. This pole mass is then used as input parameter m in Eq. (33) to determine the PS and $\overline{\rm PS}$ masses at LO, NLO, and NNLO. The obtained values for the PS and $\overline{\rm PS}$ mass differ only in NNLO. The results of these calculations are collected in Table 1, together with the estimates for "large β_0" accuracy [49,59]. Note that the same values for the $\overline{\rm MS}$ mass have been used for Tables 2 and 3 in Ref. [29]. The obtained mass values can now be used for the analysis in the following section.

Taking the $\overline{\rm PS}$ mass instead of the PS mass, we observe an improvement of the convergence. The differences for the mass values in going from LO to NLO to NNLO to the "large β_0" estimate for e.g. $\overline{m}(\overline{m}) = 165\,{\rm GeV}$ read $7.64\,{\rm GeV}$, $1.64\,{\rm GeV}$, $0.52\,{\rm GeV}$, and $0.25\,{\rm GeV}$ for the pole mass, $6.72\,{\rm GeV}$, $1.21\,{\rm GeV}$, $0.29\,{\rm GeV}$, and $0.08\,{\rm GeV}$ for the PS mass and finally $6.72\,{\rm GeV}$, $1.21\,{\rm GeV}$, $0.27\,{\rm GeV}$, and $0.08\,{\rm GeV}$ for the $\overline{\rm PS}$ mass.

In Fig. 4 we show the difference between the $\overline{\rm PS}$ and the PS mass (in GeV) as a function of the factorization scale μ_f (solid line) at $\mu = 15\,{\rm GeV}$. It is interesting to observe that the non-abelian part of the difference between the $\overline{\rm PS}$ and the PS mass (dotted line in Fig. 4) can be as large as $200\,{\rm MeV}$. But the recoil correction cancel in part the non-abelian one and therefore the final difference is not more than $50\,{\rm MeV}$. The dependence of $m_{\overline{\rm PS}} - m_{\rm PS}$ on the renormalization scale at $\mu_f = 30\,{\rm GeV}$ is given in Fig. 4 by the dashed curve.

4 NNLO results

4.1 The scheme with the pole mass

The top quark cross section at LO, NLO, and NNLO is shown in Fig. 5 as a function of the center-of-mass energy. For the top quark pole mass we use $m_t = 175.05\,{\rm GeV}$, for the top quark width $\Gamma_t = 1.43\,{\rm GeV}$, and for the QCD coupling constant $\alpha_s(m_Z) = 0.119$ [60]. Different values $\mu = 15\,{\rm GeV}$, $30\,{\rm GeV}$, and $60\,{\rm GeV}$ for the renormalization scale are selected because they roughly

$\overline{m}(\overline{m})$	$m_{\rm PS}^{\rm LO}$	$m_{\rm PS}^{\rm NLO}$	$m_{\rm PS}^{\rm NNLO}$ $m_{\overline{\rm PS}}^{\rm NNLO}$	$m_{\rm PS}^{\beta_0}$ $m_{\overline{\rm PS}}^{\beta_0}$	$m_{\rm pole}^{\rm LO}$	$m_{\rm pole}^{\rm NLO}$	$m_{\rm pole}^{\rm NNLO}$	$m_{\rm pole}^{\beta_0}$
160.0	166.51	167.69	167.97 167.95	168.05 168.03	167.44	169.05	169.56	169.80
165.0	171.72	172.93	173.22 173.20	173.30 173.28	172.64	174.28	174.80	175.05
170.0	176.92	178.17	178.47 178.45	178.55 178.53	177.84	179.52	180.05	180.30

Table 1: Top quark mass relations for the $\overline{\rm MS}$, PS, $\overline{\rm PS}$, and the pole mass at LO, NLO, NNLO, and "large β_0" accuracy in GeV. We fix the $\overline{\rm MS}$ mass to be $\overline{m}(\overline{m}) = 160\,{\rm GeV}$, 165 GeV, and 170 GeV and find the pole mass at LO, NLO, and NNLO from the three-loop relation in Eq. (38). The PS and $\overline{\rm PS}$ masses are derived from the pole mass by using Eq. (33) (without or with the $1/m$ contributions, respectively). We use the QCD coupling constant $\alpha_s(m_Z) = 0.119$, $\mu = \overline{m}(\overline{m})$, and $\mu_f = 20\,{\rm GeV}$ for the factorization scale in the PS and $\overline{\rm PS}$ masses.

correspond to the typical spatial momenta for the top quark. For solving the Schrödinger equation we use the program written by one of the authors [24]. Note that we do not take into account an initial photon radiation which would change the shape of the cross section. This can be easily included in the Monte Carlo simulation.

The NNLO curve modifies the line shape by the amount of $20-30\%$ which is as large as the NLO correction. It also shifts the position of the $1S$ peak by approximately 600 MeV. These large shifts of the peak position were expected. As we discussed above (and is well-known in the literature [30,31]), the pole mass definition suffers from the renormalon ambiguity. The top quark pole mass cannot be defined better than $O(\Lambda_{\rm QCD})$. Large NNLO corrections and a large shift of the $1S$ resonance can spoil the top quark mass measurement at the NLC.

4.2 The scheme with the PS mass

In this subsection we discuss the calculation scheme using the PS mass. We redefine the pole mass through the PS mass using the relation given in Eq. (33) without the $1/m$ contributions and then use the PS mass as an input parameter for our numerical analysis at LO, NLO, and NNLO. In Fig. 6 we show the top quark cross section expressed in terms of $m_{\rm PS}(\mu_f)$ at LO, NLO, and NNLO (like in Fig. 5) as a function of the center-of-mass energy. We take $m_{\rm PS}(\mu_f = 20\,{\rm GeV}) = 173.30\,{\rm GeV}$ which corresponds to the pole mass $m = 175.05\,{\rm GeV}$ according to Table 1. In looking at Fig. 6 we observe an improvement in the stability of the position of the first peak in comparison to the previous analysis as we go from LO to NLO to NNLO. Actually, for the three values $\mu = 15\,{\rm GeV}$, $30\,{\rm GeV}$, and $60\,{\rm GeV}$ we obtain the maxima of the $1S$ peak for NNLO at $s_{\rm max} = 347.32\,{\rm GeV}$, $347.41\,{\rm GeV}$, and $347.48\,{\rm GeV}$ while the maximal values are given by $R_{\rm max} = 1.379$, 1.184, and 1.088, respectively. This demonstrated that a large variation in the renormalization scale μ gives rise only to a shift of about $160\,{\rm MeV}$ for the $1S$ peak position at NNLO while the variation for $R_{\rm max}$ is still large.

4.3 The scheme with the $\overline{\rm PS}$ *mass*

In this subsection we discuss the calculation scheme where we use the $\overline{\rm PS}$ mass. We redefine the pole mass through the $\overline{\rm PS}$ mass by using the relation given in Eq. (33) and then use the $\overline{\rm PS}$ mass as an input parameter for the numerical analysis at LO, NLO, and NNLO. In Fig. 7 we show the top quark cross section expressed in terms of $m_{\overline{\rm PS}}(\mu_f)$ at LO, NLO, and NNLO (like in Fig. 5) as a function of the center-of-mass energy. We take $m_{\overline{\rm PS}}(\mu_f = 20\,{\rm GeV}) = 173.28\,{\rm GeV}$. Again we observe a very good stability of the position of the first peak as we go from LO to NLO to NNLO, similar to the one observed for the PS mass case. Studying the size of the NNLO corrections to the peak positions we conclude that the current theoretical uncertainty of the determination of the PS mass from the $1S$ peak position is about $100 - 200\,{\rm MeV}$.

5 Conclusion and discussions

We discussed the so-called potential subtracted (PS) mass suggested in Ref. [32] as a definition of the quark mass alternative to the pole mass. In contrast to the pole mass, this mass is not sensitive to the non-perturbative QCD effects. We have derived recoil corrections to the relation of the pole mass with the PS mass. The main result for this is Eq. (33). In addition, we demonstrated that, if we use the PS or the $\overline{\rm PS}$ mass in the calculations, the perturbative predictions for the cross section become much more stable at higher orders of QCD (shifts are below $0.1\,{\rm GeV}$). This understanding removes one of the obstacles for an accurate top mass measurement and one can expect that the top quark mass will be extracted from a threshold scan at NLC with an accuracy of about $100 - 200\,{\rm MeV}$.

Acknowledgements: We are grateful to R. Akhoury, E. Yao, M. Beneke,

A. Hoang, D. Gerdes, and U. Bauer for valuable discussions. O.Y. acknowledges support from the US Department of Energy (DOE). S.G. acknowledges a grant given by the DFG, FRG, he also would like to thank the members of the theory group at the Newman Lab for their hospitality during his stay.

References

1. F. Abe *et al.* [CDF Collaboration],
   Phys. Rev. Lett. **74** (1995) 2626 [hep-ex/9503002]
   S. Abachi *et al.* [D0 Collaboration],
   Phys. Rev. Lett. **74** (1995) 2632 [hep-ex/9503003]
2. G. Brooijmans [CDF and D0 Collaborations],
   "Top quark mass measurements at the Tevatron" [hep-ex/0005030]
3. M.E. Peskin, "Physics goals of the linear collider" [hep-ph/9910521]
4. V.S. Fadin and V.A. Khoze, JETP Lett. **46** (1987) 525
5. V.S. Fadin and V.A. Khoze, Sov. J. Nucl. Phys. **48** (1988) 309
6. E.C. Poggio, H.R. Quinn and S. Weinberg, Phys. Rev. **D13** (1976) 1958
7. M.J. Strassler and M.E. Peskin, Phys. Rev. **D43** (1991) 1500
8. V.S. Fadin and O. Yakovlev, Sov. J. Nucl. Phys. **53** (1991) 688
9. W. Kwong, Phys. Rev. **D43** (1991) 1488
10. M. Jeżabek, J.H. Kühn and T. Teubner, Z. Phys. **C56** (1992) 653
11. Y. Sumino, K. Fujii, K. Hagiwara, H. Murayama and C.K. Ng,
    Phys. Rev. **D47** (1993) 56
12. R.J. Guth and J.H. Kühn, Nucl. Phys. **B368** (1992) 38
13. W. Beenakker and W. Hollik, Phys. Lett. **269 B** (1991) 425
14. V.S. Fadin and O. Yakovlev, Sov. J. Nucl. Phys. **53** (1991) 1053;
    Sov. J. Nucl. Phys. **50** (1989) 1037
15. K. Melnikov and O. Yakovlev,
    Phys. Lett. **324 B** (1994) 217 [hep-ph/9302311]
16. V.S. Fadin, V.A. Khoze and A.D. Martin, Phys. Rev. **D49** (1994) 2247
17. V.S. Fadin, V.A. Khoze and A.D. Martin,
    Phys. Lett. **320 B** (1994) 141 [hep-ph/9309234]
18. Y. Sumino, PhD thesis, 1993
19. K. Melnikov and O. Yakovlev, "Radiative interference effects in the top production," Proceedings of the Physics with e+ e- Linear Colliders (The European Working Groups 4 Feb - 1 Sep 1995: Session 3), Hamburg, Germany, 30 Aug - 1 Sep 1995; In "Annecy/Gran Sasso/Hamburg 1995: e^+e- collisions at TeV energies" 21-28, DESY, Hamburg, Report No. DESY-96-123-D, pages 21–28
20. K. Melnikov and O. Yakovlev, "On the precise description of the reactions

with the unstable particles," Proceedings of the Workshop on Heavy Quarks, Bad Honnef, Germany, 14–17 Dec 1994, pages 165–170
21. K. Melnikov and O. Yakovlev, Nucl. Phys. **B471** (1996) 90 [hep-ph/9501358]
22. A.H. Hoang and T. Teubner, Phys. Rev. **D58** (1998) 114023 [hep-ph/9801397]
23. K. Melnikov and A. Yelkhovsky, Nucl. Phys. **B528** (1998) 59 [hep-ph/9802379]
24. O. Yakovlev, Phys. Lett. **457 B** (1999) 170 [hep-ph/9808463]
25. M. Beneke, A. Signer and V.A. Smirnov, Phys. Lett. **454 B** (1999) 137 [hep-ph/9903260]
26. A.H. Hoang and T. Teubner, Phys. Rev. **D60** (1999) 114027 [hep-ph/9904468]
27. T. Nagano, A. Ota and Y. Sumino, Phys. Rev. **D60** (1999) 114014 [hep-ph/9903498]
28. A.A. Penin and A.A. Pivovarov, "Analytical results for $e^+e^- \to t\bar{t}$ and $\gamma\gamma \to t\bar{t}$ observables near the threshold up to the next-to-next-to-leading order of NRQCD" [hep-ph/9904278]
29. A.H. Hoang *et al.*, Eur. Phys. J. **C3** (2000) 1
30. M. Beneke and V.M. Braun, Nucl. Phys. **B426** (1994) 301 [hep-ph/9402364]
31. I.I. Bigi, M.A. Shifman, N.G. Uraltsev and A.I. Vainshtein, Phys. Rev. **D50** (1994) 2234 [hep-ph/9402360]
32. M. Beneke, Phys. Lett. **434 B** (1998) 115 [hep-ph/9804241]
33. N. Uraltsev, "Heavy-quark expansion in beauty and its decays", talk given at the International School of Physics, "Enrico Fermi: Heavy Flavor Physics – A Probe of Nature's Grand Design", Varenna, Italy, July 8–18, 1997, In "Varenna 1997, Heavy flavor physics", p. 329 [hep-ph/9804275]
34. A. Czarnecki, K. Melnikov and N. Uraltsev, Phys. Rev. Lett. **80** (1998) 3189 [hep-ph/9708372]
35. A.H. Hoang and T. Teubner, Phys. Rev. **D60** (1999) 114027 [hep-ph/9904468]
36. O. Yakovlev, talk given at the Mini-Workshop on "Physics at the $t\bar{t}$ threshold", Karlsruhe, Germany, Dec. 20, 1998; talk given at the Workshop on "Physics at NLC", Berkeley, California, March 2000.
37. K. Melnikov, talk given at the Mini-Workshop on "Physics at the $t\bar{t}$ threshold", Karlsruhe, Germany, Dec. 20, 1998.
38. O. Yakovlev and S. Groote, "Top quark mass definition and $t\bar{t}$ production near threshold at the NLC" [hep-ph/0008156]
39. R. Karplus and A. Klein, Phys. Rev. **87** (1952) 848

40. A. Billoire, Phys. Lett. **92 B** (1980) 343
41. W.E. Caswell and G.P. Lepage, Phys. Lett. **167 B** (1986) 437
42. G.T. Bodwin, E. Braaten and G.P. Lepage,
    Phys. Rev. **D51** (1995) 1125 [hep-ph/9407339]
43. A. Pineda and J. Soto, Phys. Rev. **D59** (1999) 016005 [hep-ph/9805424]
44. A. Czarnecki and K. Melnikov,
    Phys. Rev. Lett. **80** (1998) 2531 [hep-ph/9712222]
45. M. Beneke and V.A. Smirnov,
    Nucl. Phys. **B522** (1998) 321 [hep-ph/9711391];
    M. Beneke, A. Signer and V.A. Smirnov,
    Phys. Rev. Lett. **80** (1998) 2535 [hep-ph/9712302]
46. A.H. Hoang, Phys. Rev. **D56** (1997) 5851; Phys. Rev. **D57** (1998) 1615
47. A.H. Hoang, M.C. Smith, T. Stelzer and S. Willenbrock,
    Phys. Rev. **D59** (1999) 114014 [hep-ph/9804227]
48. Y. Sumino, "Renormalon cancellation in heavy quarkonia and determination of m_b, m_t" [hep-ph/0004087]
49. U. Aglietti and Z. Ligeti, Phys. Lett. **364 B** (1995) 75 [hep-ph/9503209]
50. M. Beneke, "Renormalons", Phys. Rept. **317** (1999) 1 [hep-ph/9807443]
51. A.A. Penin and A.A. Pivovarov,
    Phys. Lett. **401 B** (1997) 294 [hep-ph/9612204];
    N.V. Krasnikov and A.A. Pivovarov,
    Mod. Phys. Lett. **A11** (1996) 835 [hep-ph/9602272];
    N.V. Krasnikov and A.A. Pivovarov, "Running coupling at small momenta, renormalization schemes and renormalons" [hep-ph/9510207]
52. S.N. Gupta and F. Radford,
    Phys. Rev. **D24** (1981) 2309; **D25** (1982) 3430;
    S.N. Gupta, F. Radford and W.W. Repko,
    Phys. Rev. **D26** (1982) 3305
53. A. Duncan, Phys. Rev. **D13** (1973) 2866
54. W. Fischler, Nucl. Phys. **B129** (1977) 157
55. M. Peter, Nucl. Phys. **B501** (1997) 471
56. Y. Schröder, Phys. Lett. **447 B** (1999) 321
57. K. Melnikov and T. van Ritbergen,
    Phys. Lett. **482 B** (2000) 99 [hep-ph/9912391]
58. K.G. Chetyrkin and M. Steinhauser,
    Phys. Rev. Lett. **83** (1999) 4001 [hep-ph/9907509];
    Nucl. Phys. **B573** (2000) 617 [hep-ph/9911434]
59. M. Beneke and V.M. Braun,
    Phys. Lett. **348 B** (1995) 513 [hep-ph/9411229]
60. Particle Data Group (C. Caso *et al.*), Eur. Phys. J. **C3** (1998) 1

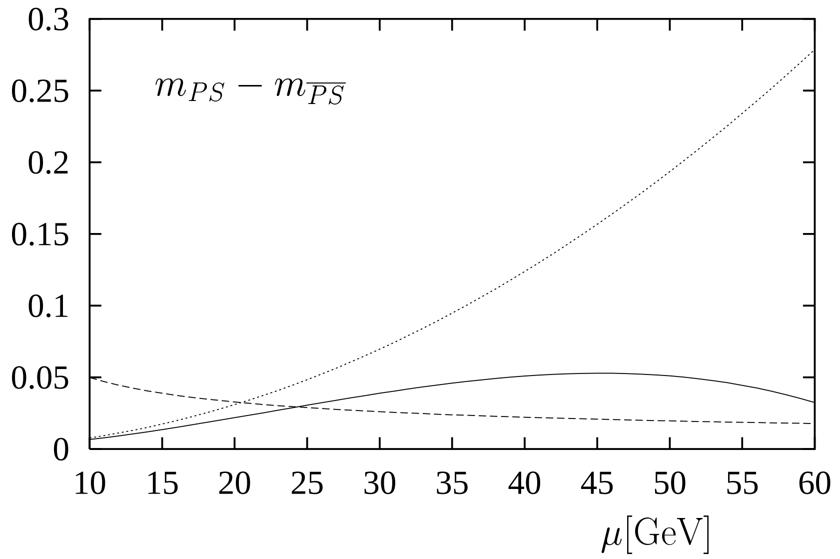

Figure 4: The difference between the PS and the $\overline{\mathrm{PS}}$ mass (in GeV) as a function of the factorization scale μ_f (solid line) at $\mu = 15\,\mathrm{GeV}$. The dotted line shows only the non-abelian part of the difference. The dependence of $m_{\overline{\mathrm{PS}}} - m_{\mathrm{PS}}$ as a function of the normalization scale μ at $\mu_f = 30\,\mathrm{GeV}$ is shown as dashed line.

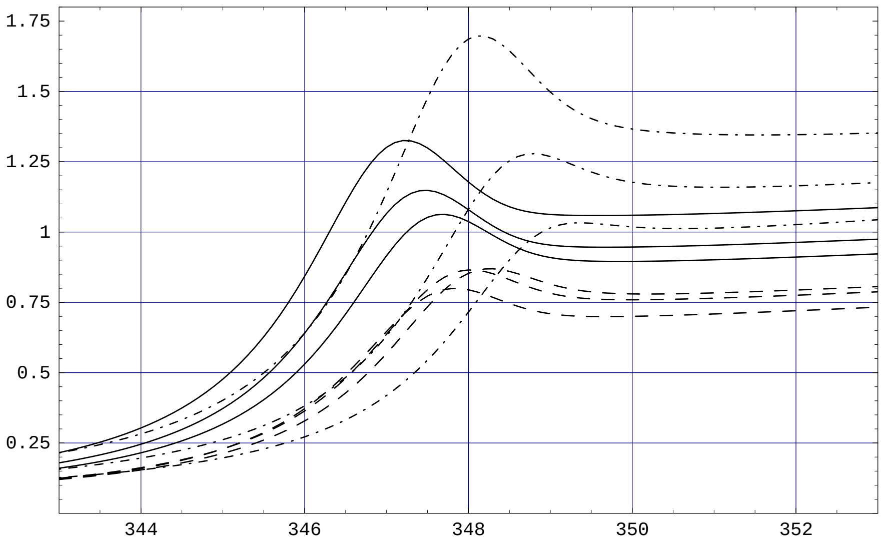

Figure 5: The scheme using the pole mass: shown is the relative cross section $R(e^+e^- \to t\bar{t})$ as a function of the center-of-mass energy in GeV for the LO (dashed-dotted lines), NLO (dashed lines), and NNLO (solid lines) approximation. We take the value $m_t = 175.05\,\mathrm{GeV}$ for the pole mass of the top quark, $\Gamma_t = 1.43\,\mathrm{GeV}$ for the top quark width, $\alpha_s(m_Z) = 0.119$ and different values $\mu = 15\,\mathrm{GeV}$, $30\,\mathrm{GeV}$, and $60\,\mathrm{GeV}$ for the renormalization scale.

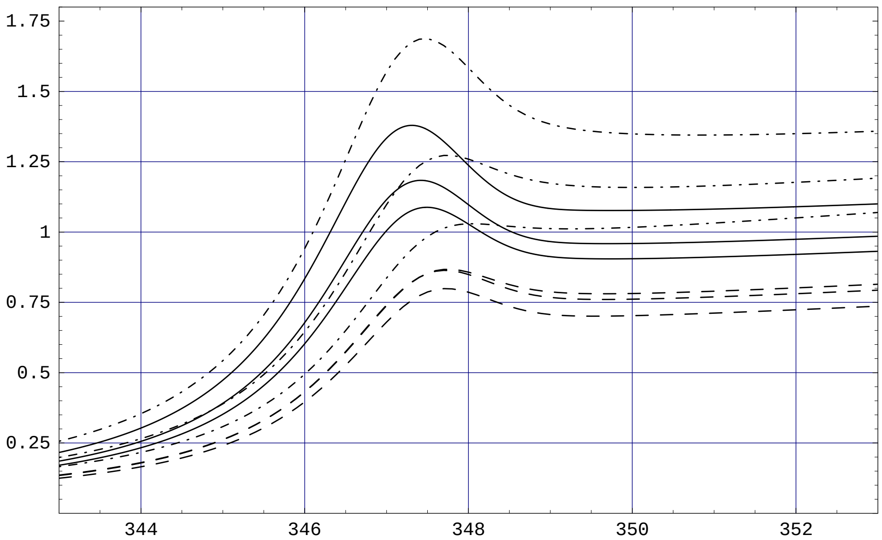

Figure 6: The scheme using the PS mass: shown is the relative cross section $R(e^+e^- \to t\bar{t})$ as a function of the center-of-mass energy in GeV for the LO (dashed-dotted lines), NLO (dashed lines), and NNLO (solid lines) approximation. We take the value $m_{\rm PS} = 173.30$ GeV for the PS mass of the top quark, $\Gamma_t = 1.43$ GeV for the top quark width, $\alpha_s(m_Z) = 0.119$ and different values $\mu = 15$ GeV, 30 GeV, and 60 GeV for the renormalization scale.

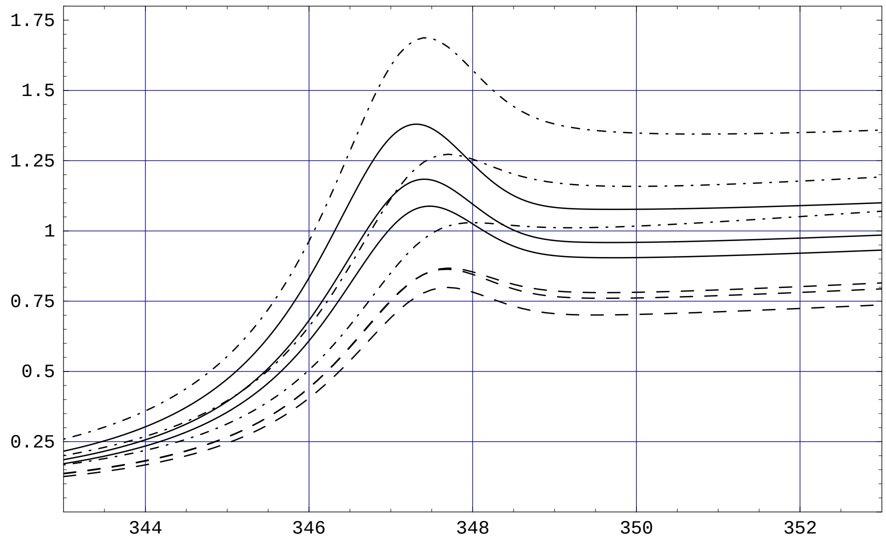

Figure 7: The scheme using the $\overline{\rm PS}$ mass: shown is the relative cross section $R(e^+e^- \to t\bar{t})$ as a function of the center-of-mass energy in GeV for the LO (dashed-dotted lines), NLO (dashed lines), and NNLO (solid lines) approximation. We take the value $m_{\overline{\rm PS}} = 173.28\,\mathrm{GeV}$ for the $\overline{\rm PS}$ mass of the top quark, $\Gamma_t = 1.43\,\mathrm{GeV}$ for the top quark width, $\alpha_s(m_Z) = 0.119$ and different values $\mu = 15\,\mathrm{GeV}$, $30\,\mathrm{GeV}$, and $60\,\mathrm{GeV}$ for the renormalization scale.